

## Article

# $^{87}\text{Sr}/^{86}\text{Sr}$ Isotopic Ratio of Ferromanganese Crusts as a Record of Detrital Influx to the Western North Pacific Ocean

Keishiro Azami <sup>1,\*</sup>, Naoto Hirano <sup>2</sup>, Jun-Ichi Kimura <sup>3</sup>, Qing Chang <sup>3</sup>, Hirochika Sumino <sup>4</sup>, Shiki Machida <sup>5</sup>, Kazutaka Yasukawa <sup>6,7</sup> and Yasuhiro Kato <sup>5,7</sup>

- <sup>1</sup> Graduate School of Science, Tohoku University, Aramaki-aoba 6-3, Aoba-ku, Sendai 980-8578, Japan
  - <sup>2</sup> Center for Northeast Asian Studies, Tohoku University, Kawauchi 41, Aoba-ku, Sendai 980-8576, Japan; nhirano@tohoku.ac.jp
  - <sup>3</sup> Japan Agency for Marine-Earth Science and Technology (JAMSTEC), Natsushima-cho 2-15, Kanagawa, Yokosuka 237-0061, Japan; jkimura@jamstec.go.jp (J.-I.K.); qchang@jamstec.go.jp (Q.C.)
  - <sup>4</sup> Research Center for Advanced Science and Technology, The University of Tokyo, Komaba 4-6-1, Meguro-ku, Tokyo 153-8904, Japan; sumino@igl.c.u-tokyo.ac.jp
  - <sup>5</sup> Ocean Resources Research Center for Next Generation, Chiba Institute of Technology, 2-17-1 Tsudanuma, Chiba, Narashino 275-0016, Japan; shiki.machida@p.chibakoudai.jp (S.M.); ykato@sys.t.u-tokyo.ac.jp (Y.K.)
  - <sup>6</sup> Frontier Research Center for Energy and Resources, School of Engineering, The University of Tokyo, Bunkyo-ku, Tokyo 113-8656, Japan; k-yasukawa@sys.t.u-tokyo.ac.jp
  - <sup>7</sup> Department of Systems Innovation, School of Engineering, The University of Tokyo, 7-3-1 Hongo, Bunkyo-ku, Tokyo 113-8656, Japan
- \* Correspondence: k.azami@aoni.waseda.jp; Tel.: +81-3-5286-3318  
† Present address: School of Creative Science and Engineering, Waseda University, 3-4-1 Okubo, Shinjuku-ku, Tokyo 169-8555, Japan.



**Citation:** Azami, K.; Hirano, N.; Kimura, J.-I.; Chang, Q.; Sumino, H.; Machida, S.; Yasukawa, K.; Kato, Y.  $^{87}\text{Sr}/^{86}\text{Sr}$  Isotopic Ratio of Ferromanganese Crusts as a Record of Detrital Influx to the Western North Pacific Ocean. *Minerals* **2022**, *12*, 943. <https://doi.org/10.3390/min12080943>

Academic Editor: Francisco J. González

Received: 4 July 2022

Accepted: 25 July 2022

Published: 27 July 2022

**Publisher's Note:** MDPI stays neutral with regard to jurisdictional claims in published maps and institutional affiliations.



**Copyright:** © 2022 by the authors. Licensee MDPI, Basel, Switzerland. This article is an open access article distributed under the terms and conditions of the Creative Commons Attribution (CC BY) license (<https://creativecommons.org/licenses/by/4.0/>).

**Abstract:** In this study, the Sr isotope ratios (IRs;  $^{87}\text{Sr}/^{86}\text{Sr}$ ) of ferromanganese (Fe–Mn) crusts are analyzed through laser ablation inductively coupled plasma multiple-collector mass spectrometry. A sample collected from off Minamitorishima Island showed uniform Sr IRs (0.70906–0.70927) similar to that of present-day seawater with more than 36 mm thickness. Meanwhile, a detritus-rich sample collected from off northeast (NE) Japan showed a wide variation in Sr IRs (0.707761–0.709963). The Sr IR variation in the Fe–Mn crust from off NE Japan suggests detrital influx contributions from both the NE Japan arc (<0.708) and aeolian dust from China (>0.718). Detrital flux from the NE Japan arc increases from the bottom to middle layers, possibly due to the uplift of the Ou backbone range that occurred after ~2 Ma. The increased influx of the aeolian dust in the outer layer is attributable to global cooling in the Quaternary that increased the loess dust transportation from China to the western North Pacific Ocean. Meanwhile, the influence of the detrital influx on the sample from off Minamitorishima Island appeared to be negligible. The Sr IR analysis with high spatial resolution proposed in this study possibly improves the burial history of Fe–Mn nodules.

**Keywords:** western North Pacific; paleoceanography; ferromanganese crust; ferromanganese nodule; Sr isotope ratio

## 1. Introduction

Submarine Fe–Mn crusts and nodules are chemical sedimentary rocks mainly comprising Fe and Mn (oxyhydr)oxides with a small amount of detrital materials (e.g., [1]) that record paleoenvironmental information about the ocean (e.g., [2–6]). They simultaneously provide geochronological information based on the variations in their chemical (e.g., Co content) and isotopic (e.g.,  $^{10}\text{Be}/^9\text{Be}$  and  $^{187}\text{Os}/^{188}\text{Os}$ ) compositions [7–10]. Several scholars have tried determining the depositional ages of Fe–Mn crusts using Sr isotope ratios (IRs;  $^{87}\text{Sr}/^{86}\text{Sr}$ ) because the Sr isotope composition of seawater varies with age [11–13]. However, they did not succeed due to the exchange of Sr with ambient seawater [14]. For example, unleached bulk Sr IRs of Fe–Mn crusts and nodules containing minimal detrital

materials show similar values with present-day seawater (0.70916; [15]) regardless of their formation ages [13,16].

Fe–Mn crusts contain detrital materials existing in marine sediments without exception. The provenance and influxes of these detrital materials have been estimated using mineral assemblages, chemical compositions, and Nd and Sr isotopic compositions to detect geological events and climate changes. Arid climates in Asia associated with global cooling have been discussed on the basis of the provenance and fraction of aeolian dust influx recorded in marine sediments from the Pacific Ocean [17–19]. However, marine sediments occasionally lack this information because of depositional hiatus or erosion. Moreover, after their formation, Fe–Mn crusts are harder to be eroded than marine sediments and can even grow in an environment of sedimentary hiatus, preserving original geochemical information, unless significant resorption otherwise occurs with an oxidation of the deep-sea environment (e.g., the phosphatization of Fe–Mn crusts on the central Pacific seamounts from the latest Eocene to the Early Oligocene [20,21]). Therefore, Fe–Mn crusts are expected to supplement the paleoenvironmental records of deep-sea sediments.

The Sr and Nd isotopic and mineral compositions of the separated detritus in Fe–Mn crusts are discussed regarding the Himalayan uplift [22] and paleoclimate in North Africa [23] from the provenance of silicate detritus and its accumulation rate. The bulk Sr isotopic ratio of Fe–Mn crusts must be a combination of the Fe–Mn oxide phase (same with present-day seawater) and detrital fluxes. Hence, the provenance and influence of detrital fluxes can be discussed on the basis of the bulk Sr IRs of Fe–Mn crusts.

Given the above background, we analyze the bulk Sr IRs ( $^{87}\text{Sr}/^{86}\text{Sr}$ ) of two contrasting Fe–Mn crusts collected from off northeast (NE) Japan and off Minamitorishima (Marcus) Island in the western North Pacific Ocean. Laser ablation multiple-collector inductively coupled plasma mass spectrometry (LA-MC-ICP-MS) with 200  $\mu\text{m}$  spatial resolution in both diameter and depth is used in this analysis. This method can measure bulk Sr IRs with 10 times higher spatial (i.e., temporal) resolution than that of previous studies, targeting slices of a few millimeters' thickness perpendicular to the growth layers of Fe–Mn crusts. In order to discuss the provenance of detrital materials from bulk Sr IRs of Fe–Mn crusts, it is suitable to analyze the samples without carbonates because carbonates enriched in Sr and holding Sr IR at the time of formation make discussion complex. In a previous study analyzing bulk Sr IRs of carbonate-rich Fe–Mn nodules from shallower than carbonate compensation depth (CCD) using LA-MC-ICP-MS [24], probably due to the existence of carbonates, the temporal Sr IR variation in the sample was interpreted confusingly as a variation of Fe–Mn oxides' Sr IRs, which should be overprinted by the Sr IRs of ambient seawater of the present day regardless of the formation age of the layers (i.e., constant value). Therefore, in this study, we discuss the provenance and temporal variation in detrital fluxes in the Fe–Mn crusts collected from deeper than CCD based on Sr IRs.

## 2. Materials and Methods

The Fe–Mn crusts were collected from petit-spot volcanoes off NE Japan (6K#1389-R07) and off Minamitorishima Island (6K#1201-R04) in the western North Pacific (Figure 1 and Table 1) via dives 6K#1389 and 6K#1201 of the submersible *SHINKAI 6500* during cruises YK14-05 and YK10-05 of R/V Yokosuka, performed by the Japan Agency for Marine–Earth Science and Technology (JAMSTEC). The petit-spot volcano which 6K#1389-R07 grew on was located on the outer rise associated with the Japan Trench, less than 400 km from NE Japan where petit-spot volcanoes were first reported [25]. On the other hand, the petit-spot volcano which 6K#1201-R04 grew on was located approximately 100 km southeast of Minamitorishima Island where several petit-spot volcanoes have been reported [26] in the North Pacific Gyre far from the continent. The thicknesses of the Fe–Mn oxide layers of 6K#1389-R07 and 6K#1201-R04 were 32 mm and 36 mm, respectively. Petit-spot volcanoes are small volcanoes (< a few km) that occur on plate flexure, particularly around the outer rise of the oceanic plate before subduction [25,26]. Therefore, the Fe–Mn crusts from these volcanoes have hydrogenetic origin without the phosphatization reported in Fe–Mn

crusts older than the Early Oligocene collected from shallower than a few km deep [20,21], and are characterized by the submarine environment at depths of 5300–6000 m due to the appearance of petit-spot volcanoes on the outer rise [27]. Considering that the CCD in the western North Pacific Ocean is reported to be 4500 m deep [28], the samples in this study must be free from marine carbonate deposits at least in the layer formed in an environment resembling the present day. The substrate of the 6K#1389-R07 Fe–Mn crust (off NE Japan) was peperite (volcanic breccia), including the highly vesicular basalt of petit-spot volcanoes that erupted at an age between 0.20 and 1.33 Ma, which was estimated from the palagonitization rate of basaltic glass [29].

**Table 1.** Sample locations and mineral compositions.

Sample	Latitude	Longitude	Water Depth (m)	Mineral Composition
6K#1389-R07	37°39.40' N	145°11.96' E	5305	V, Q, Pl
L-i <sub>NEJ</sub>				V, T (minor), Q, Pl
L-ii <sub>NEJ</sub>				V, T (minor), Q, Pl
L-iii <sub>NEJ</sub>				V, T (minor), Q, Pl
6K#1201-R04	23°32.48' N	154°41.32' E	5363	V, Q, Pl
L0 <sub>MI</sub>				V, Q, Pl
L1 <sub>MI</sub>				V, Q, Pl
L2 <sub>MI</sub>				V, Q, Pl

V: vernadite, T: 10-Å manganate Q: quartz, Pl: plagioclase.

The Fe–Mn crust samples were cut into slices perpendicular to the growth surfaces and were molded into epoxy resin after being dried. The cross-section surfaces were polished dry (Figure 1B) and their Sr IRs were analyzed through multiple-collector inductively coupled plasma mass spectrometry (MC-ICP-MS) (Thermo Fisher Scientific, Neptune, Waltham, MA, USA) at JAMSTEC. For in situ Sr analysis, the Fe–Mn crusts were sampled through laser ablation (LA) with a crater diameter and depth of 200 µm using a 193 nm ArF excimer LA system (OK Laboratory, OK ExLA-3000, Mitaka, Tokyo, Japan). The analysis points were selected from the cross-section surface covered with Fe–Mn oxides under the observation of a reflection microscope attached on the LA system during the analysis. The repetition rate of the LA pulse was set to 5 and 2 Hz for 6K#1389-R07 and 6K#1201-R04, respectively, depending on the sample property. The ablated aerosols were transferred to MC-ICP-MS to determine both Sr IRs ( $^{87}\text{Sr}/^{86}\text{Sr}$ ) and relative Sr concentrations through the  $^{88}\text{Sr}$  signal intensity derived from the given crater volumes. Thus, the relative Sr concentrations of 6K#1201-R04 were normalized to be comparable to those of 6K#1389-R07 based on the ratio of the repetition rate. The Sr IRs were accurately analyzed without separating the isobaric  $^{87}\text{Rb}$  from  $^{87}\text{Sr}$  because the Rb concentrations in the Fe–Mn crusts were typically several orders of magnitude lower than Sr ( $\text{Sr}/\text{Rb} \approx 100$ ) [1]. Nevertheless, we routinely checked the  $^{87}\text{Rb}$  isobars on  $^{87}\text{Sr}$  using experimentally determined  $^{87}\text{Rb}/^{85}\text{Rb}$  ratios combined with the mass bias factor measured from the canonical ratio of  $^{86}\text{Sr}/^{88}\text{Sr} = 0.1194$ . The suppressions of  $^{84}\text{Kr}$  and  $^{86}\text{Kr}$  gas blank baselines were significant for the mass loading of sample aerosols from 200 µm craters. The blank effects on the  $^{87}\text{Sr}/^{86}\text{Sr}$  ratios were corrected by the linear relation between  $^{87}\text{Sr}/^{86}\text{Sr}$  and  $^{88}\text{Sr}/^{84}\text{Sr}$  (double correction). All analytical details are in accordance with Kimura et al.'s study [30].

In addition, we performed qualitative elemental mapping of the Mn, Fe, and K contents of the polished samples using micro-X-ray fluorescence ( $\mu\text{XRF}$ ) (Hitachi, EA6000VX, Chiyoda-ku, Tokyo, Japan) with energy-dispersive X-ray spectroscopy at JAMSTEC. The analysis conditions were as follows: accelerating voltage of 45 kV, probe current of 0.9 A, beam diameter (pixel size) of 70 or 80 µm, and scanning rate of 100 ms/pixel. Based on the chemostratigraphy obtained from the  $\mu\text{XRF}$  analysis, 6K#1389-R07 was subdivided into three layers to evaluate the bulk contents of Sr and rare-earth elements (REEs) through inductively coupled plasma mass spectrometry (ICP-MS) (Thermo Fisher Scientific, iCAP Q) at the Department of Systems Innovation, University of Tokyo, following the procedures

of Kato et al. [31] and Azami et al. [27]. The analysis yielded results generally within 5% of the accepted values for the standard materials JB-2 and JMS-2 (determined by Makishima and Nakamura [32] and Takaya et al. [33], respectively)

We also used a powder X-ray diffraction (XRD) analysis of the samples (6K#1389-R07 and 6K#1201-R04) to identify minerals. XRD analysis was performed using Ultima IV (Rigaku, Akishima, Tokyo, Japan) at the Department of Systems Innovation, University of Tokyo, with  $\text{CuK}\alpha$  radiation of 40 kV and 30 mA and scanning between  $3^\circ$  and  $75^\circ$   $2\theta$  at  $1^\circ/\text{min}$ .

The substrate 6K#1201-R04 basalt sample was subjected to  $^{40}\text{Ar}/^{39}\text{Ar}$  dating to determine the upper limit of the starting age of the Fe–Mn crust growth. The process was reasonable because the Fe–Mn crust immediately covered the quenched basalt glass rinds formed at the margin of a basalt lava flow. The separated groundmass phases from the basalt sample were crushed into 300–500  $\mu\text{m}$  grains and leached with 1N  $\text{HNO}_3$  at 60–70  $^\circ\text{C}$  for 3 h before  $^{40}\text{Ar}/^{39}\text{Ar}$  dating. The samples wrapped in Al foil were neutron-irradiated for 24 h using EB-1 biotite flux monitors [34],  $\text{K}_2\text{SO}_4$ , and  $\text{CaF}_2$  in the Kyoto University Research Reactor. During the irradiation, the samples were shielded by Cd foil to minimize the neutron-induced  $^{40}\text{Ar}$  production from  $^{40}\text{K}$  [35]. The Ar extraction and isotope analyses were performed at the Isotope Science Center, University of Tokyo. During incremental heating, gases were extracted using 11 steps between 600  $^\circ\text{C}$  and 1500  $^\circ\text{C}$ . The detailed analytical methods are described by Ebisawa et al. [36].

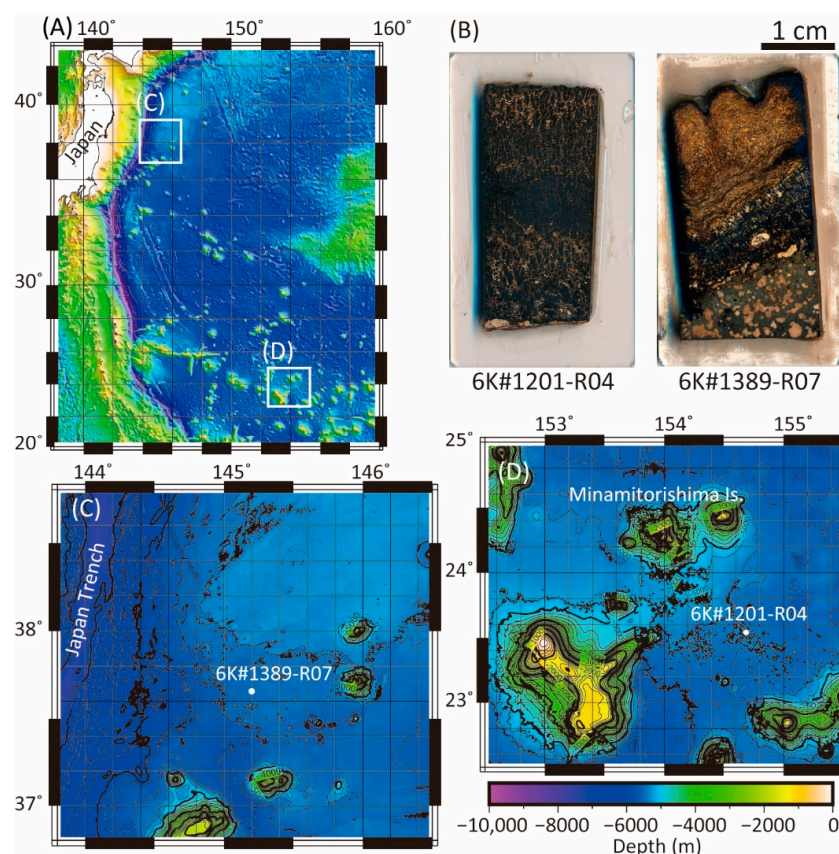


**Figure 1.** Sample locations and photos. (A) Location map showing Japan and white outline of the area shown in (C,D). (B) Photos of 6K#1201-R04 from off Minamitorishima Island and 6K#1389-R07 from off NE Japan. (C) Detailed map of off NE Japan and the sampling location (white dot). (D) Detailed map of off Minamitorishima Island and the sampling location (white dot). All maps were generated using Generic Mapping Tools software [37,38]. Bathymetric data were from ETOPO1 [39] and determined through site surveys using a multi-narrow beam echo sounder during cruises KR03-07, KR04-08, YK05-06, YK10-05, MR14-E02, MR15-E01 Legs 2 and Legs 3, and MR15-02 by JAMSTEC.

### 3. Results

Because K is typically associated with detrital materials in Fe–Mn crusts [1], its elemental map almost reflects the amount of detrital materials in the Fe–Mn crusts. Therefore, we classified the samples into three layers based on the elemental maps of K (Figure 2). The Fe–Mn crust off Minamitorishima Island (6K#1201-R04) was subdivided into a top layer with some detritus (L0<sub>MI</sub>), a middle layer with less detritus (L1<sub>MI</sub>), and a bottom layer (L2<sub>MI</sub>). These layer classifications are based on the Fe–Mn nodules off Minamitorishima Island [40] (Figure 2). The Fe–Mn crust off NE Japan (6K#1389-R07) was subdivided into the top layer that was Fe-rich (L-i<sub>NEJ</sub>), the detritus- and Mn-rich middle layer (L-ii<sub>NEJ</sub>), and the bottom layer with less detritus (L-iii<sub>NEJ</sub>), including thin detritus-rich sublayers (Figure 2; detailed views in Figure 3).

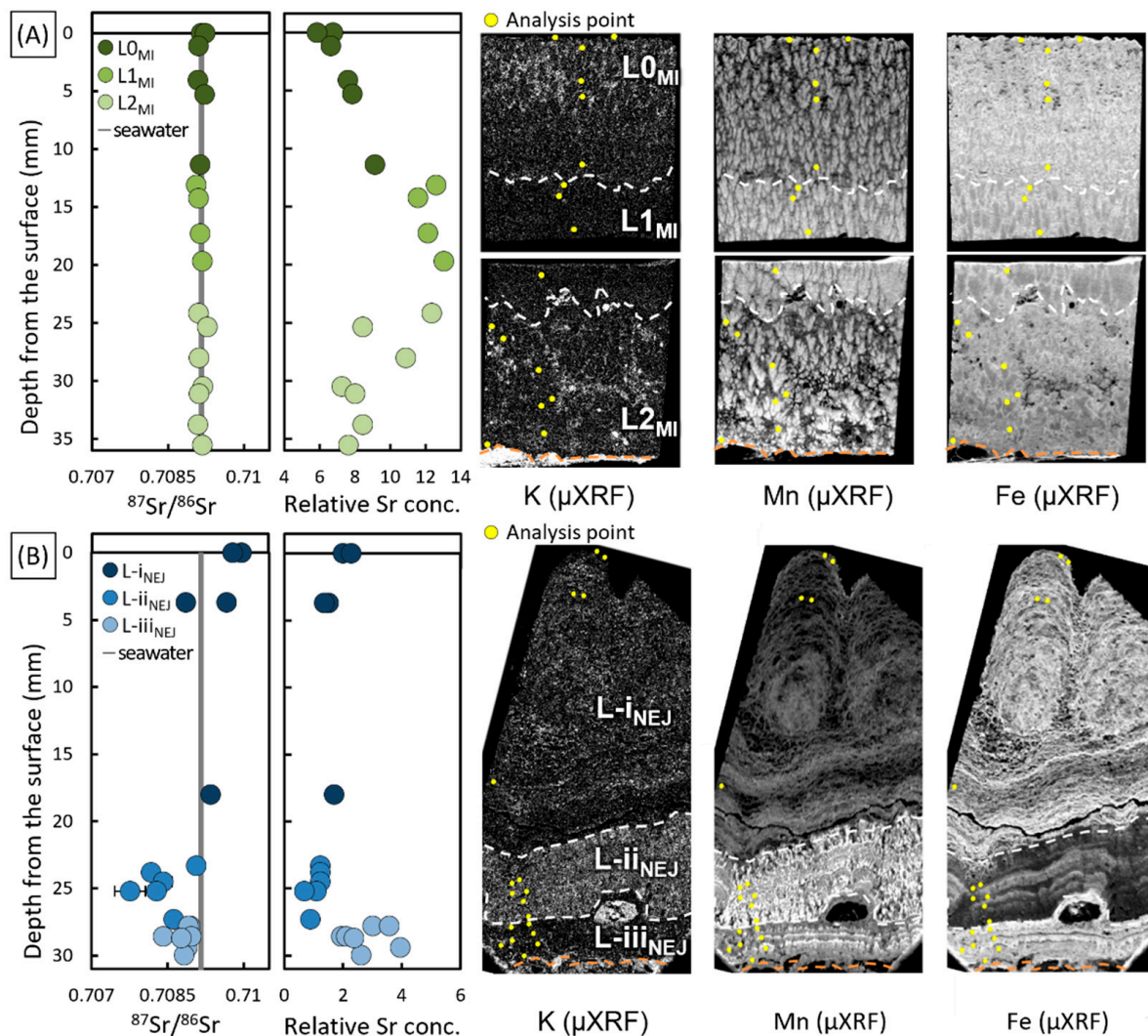


**Figure 2.** Depth profiles for Sr IRs and relative Sr concentrations with elemental maps. “Relative Sr conc.” represents the intensity of the <sup>88</sup>Sr signal. (A) Results of 6K#1201-R04 from off Minamitorishima Island. (B) Results of 6K#1389-R07 from off NE Japan. The yellow dots indicate the points analyzed by LA-MC-ICP-MS. The white- and orange-dashed lines show the boundary of layers and a boundary between the Fe–Mn crust and the substrate, respectively.

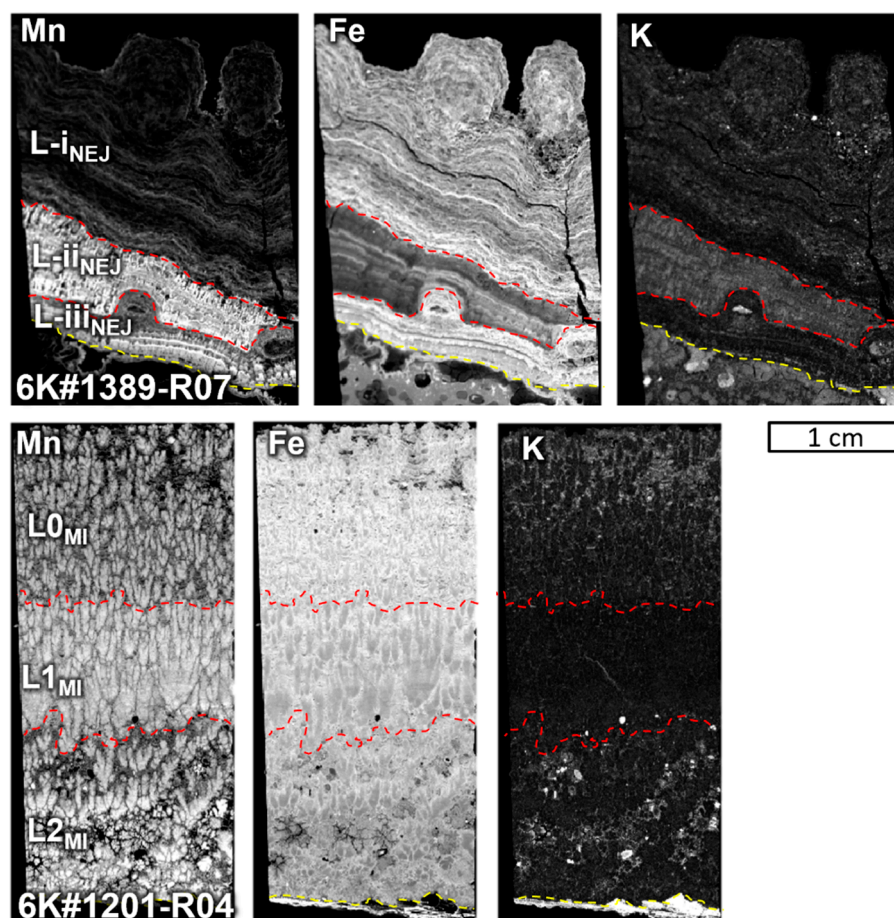


**Figure 3.** Elemental maps of Mn, Fe, and K (qualitative analysis). Both samples are subdivided into three layers based on geochemical features (details are discussed in the main text). The red- and yellow-dashed lines show the boundary of layers and a boundary between the Fe–Mn crust and substrate, respectively.

The 6K#1201-R04 from the Minamitorishima sample showed an almost constant Sr IR (0.70906–0.70927) from L0<sub>MI</sub> to L2<sub>MI</sub>, which is similar to that of present-day seawater (0.70916) [15] (Figure 2 and Table 2). The relative Sr contents (intensity of <sup>88</sup>Sr signal) of 6K#1201-R04 were high in L1<sub>MI</sub> and decreased from the bottom side to the top side in L0<sub>MI</sub>. Meanwhile, the 6K#1389-R07 from NE Japan sample exhibited higher Sr IRs in L-i<sub>NEJ</sub> (0.708864–0.709963) than that of present-day seawater. Moreover, the L-ii<sub>NEJ</sub> detritus-rich layer showed lower Sr IRs (0.707761–0.709069) and relative Sr contents than the other layers. Notably, the layer with less detritus L-iii<sub>NEJ</sub> showed higher relative Sr contents than the layers with seawater-like Sr IRs (0.708418–0.708970) (Figure 2 and Table 2). Because we analyzed Sr IRs of the sample surface covered with Fe–Mn oxides, the distribution of analysis points in detritus-rich 6K#1389-R07 became uneven, especially in L-i<sub>NEJ</sub>. The bulk Sr contents of L-i<sub>NEJ</sub>, L-ii<sub>NEJ</sub>, and L-iii<sub>NEJ</sub>, determined via ICP-MS, were 499, 415, and 771 µg/g, respectively (Table 3).

**Table 2.** Relative Sr concentrations and IRs measured by LA-MC-ICP-MS.

Sample	Relative Sr Conc.	$^{87}\text{Sr}/^{86}\text{Sr}$	$2\sigma$	Depth from the Surface (mm)
6K#1389-R07				
1389R7-1	1.990	0.70996	$7.96 \times 10^{-5}$	0
1389R7-2	2.276	0.70978	$1.01 \times 10^{-4}$	0
1389R7-3	1.507	0.70967	$1.15 \times 10^{-4}$	3.71
1389R7-4	1.365	0.70886	$9.15 \times 10^{-5}$	3.71
1389R7-5	1.695	0.70935	$9.32 \times 10^{-5}$	17.99
1389R7-6	1.222	0.70907	$1.13 \times 10^{-4}$	23.31
1389R7-7	1.236	0.70817	$1.12 \times 10^{-4}$	23.80
1389R7-8	1.221	0.70841	$1.75 \times 10^{-4}$	24.50
1389R7-9	1.089	0.70828	$1.57 \times 10^{-4}$	25.20
1389R7-10	0.688	0.70776	$3.03 \times 10^{-4}$	25.20
1389R7-11	0.895	0.70862	$1.14 \times 10^{-4}$	27.30
1389R7-12	3.001	0.70894	$4.48 \times 10^{-5}$	27.79
1389R7-13	1.934	0.70842	$1.34 \times 10^{-4}$	28.56
1389R7-14	3.939	0.70889	$3.97 \times 10^{-5}$	29.40
1389R7-15	2.615	0.70882	$6.85 \times 10^{-5}$	29.96
1389R7-20	3.564	0.70892	$4.41 \times 10^{-5}$	27.79
1389R7-21	2.116	0.70897	$1.07 \times 10^{-4}$	28.56
1389R7-22	2.381	0.70877	$6.78 \times 10^{-5}$	28.70
6K#1201-R04				
1201R04-1	6.753	0.70916	$4.21 \times 10^{-5}$	0
1201R04-2	5.844	0.70924	$6.28 \times 10^{-5}$	0
1201R04-3	6.645	0.70910	$4.04 \times 10^{-5}$	1.12
1201R04-4	7.589	0.70909	$4.79 \times 10^{-5}$	4.08
1201R04-5	7.843	0.70923	$4.33 \times 10^{-5}$	5.28
1201R04-6	9.1374	0.70914	$3.67 \times 10^{-5}$	11.36
1201R04-7	12.6147	0.70906	$2.87 \times 10^{-5}$	13.12
1201R04-8	11.585	0.70910	$2.99 \times 10^{-5}$	14.24
1201R04-9	12.121	0.70913	$3.04 \times 10^{-5}$	17.28
1201R04-10	13.0312	0.70918	$2.65 \times 10^{-5}$	19.68
1201R04-11	12.340	0.70910	$3.29 \times 10^{-5}$	24.16
1201R04-12	8.451	0.70927	$4.20 \times 10^{-5}$	25.36
1201R04-13	10.884	0.70912	$3.60 \times 10^{-5}$	28.00
1201R04-14	7.271	0.70918	$5.05 \times 10^{-5}$	30.48
1201R04-15	8.0043	0.70912	$3.26 \times 10^{-5}$	31.12
1201R04-16	8.4368	0.70909	$4.08 \times 10^{-5}$	33.76
1201R04-17	7.6341	0.70917	$4.08 \times 10^{-5}$	35.52

**Table 3.** Chemical compositions of the layers.

Sample	6K#1389-R07			6K#1201-R04		
	L-i <sub>NEJ</sub>	L-ii <sub>NEJ</sub>	L-iii <sub>NEJ</sub>	L0 <sub>MI</sub>	L1 <sub>MI</sub>	L2 <sub>MI</sub>
Mn (%)	13.5	20.0	17.3	3.9	19.2	15.4
Fe	18.7	18.7	15.0	13.7	8.3	17.7
Sr (ppm)	853	1177	969	499	415	771
Y	146	180	142	67.0	54.0	121
La	208	272	200	93.7	66.4	198
Ce	1278	1655	1414	370	347	1130
Pr	51.0	64.0	45.0	29.1	19.1	49.1
Nd	199	247	175	117	79.5	198
Sm	44.6	53.3	39.3	27.2	19.7	43.8
Eu	11.1	13.2	9.5	6.6	4.8	11.0

Table 3. Cont.

Sample	6K#1389-R07			6K#1201-R04		
	L-i <sub>NEJ</sub>	L-ii <sub>NEJ</sub>	L-iii <sub>NEJ</sub>	L0 <sub>MI</sub>	L1 <sub>MI</sub>	L2 <sub>MI</sub>
Gd	46.7	55.8	40.9	25.2	18.8	43.0
Tb	7.4	8.8	6.3	3.9	3.1	6.8
Dy	43.8	52.4	37.4	21.6	17.6	38.6
Ho	8.4	10.3	7.4	3.8	3.2	7.2
Er	23.5	28.8	21.4	10.4	9.3	20.3
Tm	3.4	4.1	3.1	1.5	1.3	2.9
Yb	22.7	26.9	20.8	9.2	8.9	19.1
Lu	3.4	4.0	3.2	1.3	1.4	2.8
Ce anomaly *	2.85	2.89	3.42	1.61	2.23	2.64
Y/Ho *	0.64	0.65	0.71	0.65	0.62	0.62

\* Normalized by Post-Archean Australian Shale.

XRD analysis identified vernadite, which is a major mineral in hydrogenetic Fe–Mn crusts, with broad peaks at approximately 2.4 and 1.4 Å, and with similar Fe–Mn minerals in the samples from both regions [1,41]. A slight 10 Å manganate was found only in the L-ii<sub>NEJ</sub> of 6K#1389-R07, which is sometimes noticed in hydrogenetic Fe–Mn crusts (e.g., [42,43]). Quartz and plagioclase were also observed in the Fe–Mn crusts from both regions. No carbonate minerals were detected.

The incremental heating <sup>40</sup>Ar/<sup>39</sup>Ar dating was performed on the groundmass separations of 6K#1201-R04 (Figure 4). Table 4 presents the age results for each fraction. The sample did not produce a clear age plateau because the three ages from 880 °C to 1000 °C, approximately equivalent within the 2σ errors, did not release <sup>39</sup>Ar higher than 50% (e.g., [44]). The higher temperature steps (>1050 °C) associated with systematically younger apparent ages are similar to those in the age spectra for the acid-leached samples of altered submarine basalts reported by Koppers et al. [45]. Therefore, the mean age, which was 36.8 ± 0.4 Ma for the three fractions from 880 °C to 1000 °C, was adopted as the eruption age of 6K#1201-R04 in further discussion.

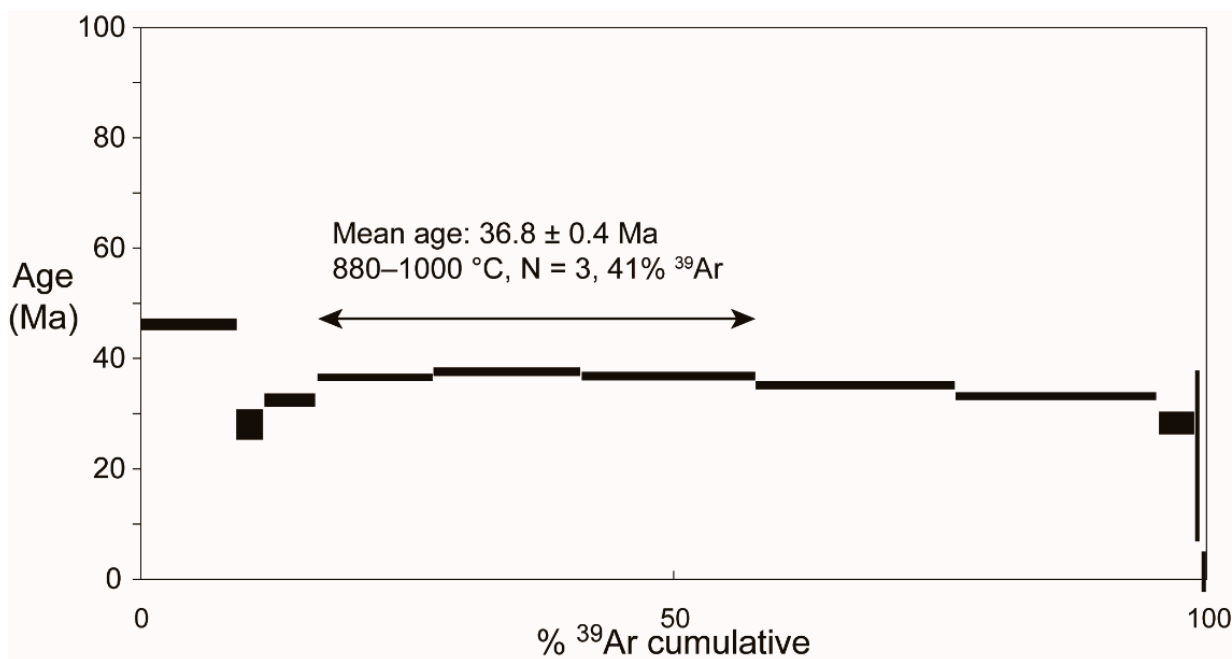


Figure 4. <sup>40</sup>Ar/<sup>39</sup>Ar age results showing the age spectrum. The errors are shown as 2σ.

**Table 4.**  $^{40}\text{Ar}/^{39}\text{Ar}$  age of 6K#1201-R04.

Fractions (°C)	$^{36}\text{Ar}/^{40}\text{Ar}$ **	$^{37}\text{Ar}/^{40}\text{Ar}$	$^{38}\text{Ar}/^{40}\text{Ar}$ **	$^{39}\text{Ar}/^{40}\text{Ar}$ **	$^{39}\text{Ar}$ (%)	Age * (Ma)
600	0.0028403 ± 0.0000056	0.0026 ± 0.0011	0.000526 ± 0.0000025	0.005341 ± 0.000011	9.0	45.96 ± 0.6
700	0.002758 ± 0.000028	0.0087 ± 0.0091	0.000562 ± 0.000012	0.010177 ± 0.000063	11.5	27.9 ± 1.3
800	0.001766 ± 0.000024	0.0278 ± 0.0077	0.000458 ± 0.000011	0.022763 ± 0.000096	16.5	32.22 ± 0.56
880	0.000496 ± 0.000017	0.0286 ± 0.0058	0.000322 ± 0.000012	0.03597 ± 0.00012	27.4	36.35 ± 0.38
950	0.000364 ± 0.000014	0.0282 ± 0.0047	0.0001886 ± 0.0000087	0.0365 ± 0.00018	41.2	37.45 ± 0.39
1000	0.000403 ± 0.000019	0.0207 ± 0.0038	0.000134 ± 0.0000072	0.036823 ± 0.000092	57.6	36.64 ± 0.38
1050	0.00047 ± 0.000015	0.028 ± 0.0039	0.00015 ± 0.00001	0.03779 ± 0.00014	76.4	34.92 ± 0.35
1120	0.000409 ± 0.000015	0.1042 ± 0.0045	0.000194 ± 0.0000082	0.04083 ± 0.0002	95.3	33.01 ± 0.35
1200	0.000707 ± 0.000088	0.895 ± 0.034	0.000305 ± 0.000035	0.04329 ± 0.00048	99.0	28.05 ± 0.99
1300	0.00162 ± 0.0006	1.83 ± 0.16	0.000392 ± 0.00025	0.0363 ± 0.0025	99.4	22.2 ± 7.6
1500	0.00365 ± 0.00022	1.898 ± 0.077	0.001138 ± 0.000066	0.01776 ± 0.00074	100.0	−6.9 ± 5.8

All data are shown by  $2\sigma$ . \*: J value is  $0.0008577 \pm 0.0000069$ , relating the production rate of  $^{39}\text{Ar}$  from  $^{39}\text{K}$ , calculated using an age standard irradiated simultaneously with the sample. \*\*: After corrections for interfering isotopes from Ca and K, which are  $(^{36}\text{Ar}/^{37}\text{Ar})_{\text{Ca}} = 0.000322 \pm 0.000017$ ,  $(^{38}\text{Ar}/^{39}\text{Ar})_{\text{K}} = 0.018203 \pm 0.000026$ , and  $(^{39}\text{Ar}/^{37}\text{Ar})_{\text{Ca}} = 0.001275 \pm 0.000027$ .  $^{40}\text{Ar}_{\text{K}}$  and  $^{38}\text{Ar}_{\text{Ca}}$  are not detected.

#### 4. Discussion

The cobalt chronometer has generally been used to estimate the growth rate of Fe–Mn crusts. However, it is inappropriate for Fe–Mn crusts near continents where cobalt flux cannot be considered constant. Therefore, the average growth rate of 6K#1389-R07 was estimated to be 24–160 mm/Myr from the thickness of the Fe–Mn oxide layer and the substrate age [29]. In general, such a high growth rate of Fe–Mn crust is associated with hydrothermal origin, although REE compositions of the samples clearly show that they are of hydrogenetic origin (Figure 5) [46]. Such a high growth rate of hydrogenetic Fe–Mn crust is not typical, except for only one report from the Arctic Ocean with a high supply of detrital materials based on radiogenic  $^{10}\text{Be}$  age (<28 mm/Myr) [47]. Therefore, the Fe–Mn crust's average growth rate would be between 24 and 28 mm/Myr limited by the substrate age and the highest growth rate of hydrogenetic Fe–Mn crusts. The 6K#1389-R07 had only been moved approximately  $1^\circ$  west along the plate motion, as estimated using GPlates software [48,49] based on the growth starting age estimated from the average growth rate and thickness (1.14–1.33 Ma) [29]. This finding demonstrates that 6K#1389-R07 had grown in almost the same geologic setting as that in the present day. Marine sediments offshore of NE Japan are influenced by aeolian dust from China and detrital materials supplied from NE Japan [17,18]. Meanwhile, the 6K#1201-R04 substrate occurred at  $178^\circ 46'$  E and  $16^\circ 27'$  N based on the  $^{40}\text{Ar}/^{39}\text{Ar}$  age ( $36.8 \pm 0.4$  Ma), indicating that the early growth layers of L2<sub>MI</sub> and L1<sub>MI</sub> (6K#1201-R04) containing less detritus would have grown in the central part of the North Pacific Gyre.

The constant Sr IRs of the 6K#1201-R04 Minamitorishima sample clearly indicate that these Fe–Mn crusts with less detritus on the present-day seafloor represent the Sr IR of present-day seawater regardless of their growth ages due to the effect of the rigorous low-temperature exchange of loosely absorbed Sr [13,16]. In contrast, the Sr IRs of the 6K#1389-R07 from the NE Japan sample varied from 0.70776 to 0.70996 (Figure 2 and Table 2) despite the almost constant seawater Sr IRs (0.7090–0.70916) during the growth of Fe–Mn crusts from approximately 1.33 Ma [15,29,50]. The variations in Sr IRs of 6K#1389-R07 were attributable to the incorporation of detrital materials, as detailed in the following discussion.

Notably, the North Pacific Ocean, including the offshore of NE Japan, has been under the influence of aeolian dust from China since at least the Late Oligocene, according to the chemical and isotopic composition of marine sediments [19]. The quartz and plagioclase in the samples are also attributable to aeolian dust because these minerals are commonly found in aeolian dust [51]. Aeolian dust from China shows high Sr IRs between 0.719 and 0.722 (values of Chinese loess at last 1.4 Myr [52]) due to the wide distribution of geological terranes as old as the Precambrian. Therefore, the elevated Sr IRs in 6K#1389-R07 higher

than that of the present-day seawater values are attributable to the effects of concomitant Chinese loess dust (Figure 2).

In the western North Pacific, the marine sediments have Sr IRs lower ( $<0.710$ ) than Chinese loess dust due to materials from the Islands of Japan [17,18]. Therefore, 6K#1389-R07 should also be influenced by the materials from NE Japan. The Quaternary volcanic products, such as widespread rhyolitic tephra in Japan, show  $<0.707$  of  $^{87}\text{Sr}/^{86}\text{Sr}$ , which is lower than the value of present-day seawater (i.e., 0.70916) [53]. However, the intermittent and short-term supplies of tephra from NE Japan are probably more difficult to be constantly recorded in Fe–Mn crusts than the continuous supply of surface debris of NE Japan due to the slow growth rate of Fe–Mn crusts. Moreover, the NE Japan side of the Pacific Ocean exhibits a low Sr IR ( $<0.709$ ) in most areas from the geochemical map of the Sr IR based on stream sediment analysis [54]. Thus, the lower Sr IRs of 6K#1389-R07 than that of present-day seawater could be explained by the contribution of the surface debris of NE Japan (including tephra fallen on land) rather than the direct supply of tephra. We verified in the following discussion that variations in Sr IRs in 6K#1389-R07 were due to both the aeolian dust from China and the detritus from NE Japan. The three-component mixing among hydrogenetic Fe–Mn oxides (seawater), aeolian dust (Chinese loess dust), and detritus from NE Japan is presented in a Sr IR diagram compared with the relative  $1/\text{Sr}$  values of the samples (Figure 6). Present-day seawater is described as having Sr IRs of hydrogenetic Fe–Mn oxides [15]. The Fe–Mn crusts from the central Pacific Ocean are described as having Sr contents of hydrogenetic Fe–Mn oxides because the Sr distributed in the detrital phase was found to be less than 0.3% of the total Sr content in the leaching experiments [55]. The weathering-resistant minerals (20% HCl residue) on the surface layer of loess sampled from the central Loess Plateau in China, which are suitable for provenance tracing in marine sediments, are described as having Sr contents and IRs of aeolian dust [51]. The surface of the marine sediments (without carbonates) in the forearc basin and landward slope of the Japan Trench [17], which were expected to have the average surface crustal composition of the Pacific Ocean side of NE Japan, were described as having detritus from NE Japan. The Sr contents of the referred materials were converted into relative Sr content simultaneously measured by LA-MC-ICP-MS using the average relative Sr content of  $L_{2\text{NEJ}}$ ; the relative Sr contents were almost constant and the Sr content of the powdered  $L_{2\text{NEJ}}$  (bulk) was measured using ICP-MS (Tables 2 and 5).

All data of the 6K#1201-R04 off Minamitorishima samples are plotted around the corner of hydrogenetic Fe–Mn oxides (Figure 6).  $L_{\text{iiiNEJ}}$  in 6K#1389-R07 from the off NE Japan samples was found in the mixing line between the hydrogenetic Fe–Mn oxides and the detritus from NE Japan. The fraction of detritus from NE Japan in terms of total Sr content increased from below 40% to approximately 80% between  $L_{\text{iiiNEJ}}$  and  $L_{\text{iiNEJ}}$ . We analyzed the sample surface covered with Fe–Mn oxides, and one data point from  $L_{\text{iiNEJ}}$  showed the NE Japan detritus as having the strongest influence (over 90% in total Sr content). This point may have been a local accumulation point of debris just below the sample surface of Fe–Mn oxides. Contrary to the change from  $L_{\text{iiiNEJ}}$  to  $L_{\text{iiNEJ}}$ , the influence of the Chinese aeolian dust increased up to 50% in total Sr content towards the outermost (present) layer of  $L_{\text{iNEJ}}$ .

The provenance of the detritus from NE Japan in 6K#1389-R07 was from the Pacific Ocean side of NE Japan, excluding the northern part (northern Kitakami Mountains) and southern part (southern Abukuma, Yamizo, and Tsukuba Mountains) due to the high Sr IRs ( $>0.7091$ ) of these areas in the geochemical map [54], explaining the low Sr IRs of the  $L_{\text{iiNEJ}}$  and  $L_{\text{iiiNEJ}}$  layers. The detritus supply from NE Japan to 6K#1389-R07 (off NE Japan) was due to the uplift event of the NE Japan arc. Based on the estimated growth rate, the Fe–Mn crust of 6K#1389-R07 started to grow between 1.14 and 1.33 Ma. After  $\sim 2$  Ma, the uplift rate of the Ou backbone range of the NE Japan arc increased rapidly, thereby increasing the detritus supply from NE Japan [56–58]. Therefore, the increase in detritus from NE Japan from  $L_{\text{iiiNEJ}}$  to  $L_{\text{iiNEJ}}$  could have been promoted by the rapid uplift of the Ou backbone range. Based on the chemical compositions of sediments in the western North Pacific, a

relative increase in volcanic components compared with aeolian dust after 2 Ma has been reported [19]. Volcanic rocks account for 38.4% of the Japanese land surface [59], and the average chemical composition of the stream and coastal marine sediments in NE Japan is similar to that of andesite, excluding highly incompatible elements, such as U and Rb [60]. Therefore, our results agree with the relative increase in volcanic components recorded in the sediments.

We suggest two factors to explain the increase in aeolian dust towards the surface of the L-i<sub>NEJ</sub> and L-ii<sub>NEJ</sub> layers: the distance change from China due to plate motion and the net increase in aeolian dust flux supplied to NE Japan offshore. In the mid-latitudes of the Pacific Ocean (30° N–45° N), the relationship between aeolian dust flux and longitude is empirically expressed as follows:

$$y = 10^{9.1 \exp(-0.007x)}, \quad (1)$$

where  $y$  and  $x$  denote the aeolian dust flux from China ( $\text{mg}/\text{cm}^2/\text{kyr}$ ) and longitude, respectively [19]. Equation (1) indicates that the aeolian dust flux is barely explained by the plate motion because 6K#1389-R07 moved only approximately 1° west during 1.33 Myr [29,48,49]. Therefore, the increase in the influence of aeolian dust from L-ii<sub>NEJ</sub> to L-i<sub>NEJ</sub> is attributable to the net increase in aeolian dust flux to NE Japan offshore. Particularly, the aeolian dust flux recorded in marine sediments exhibited an increasing trend (more than a few times) during the last 0.5 Myr in the western North Pacific, reflecting the aridification related to global cooling [61]. Assuming the same growth rate for all layers (24–28 mm/Myr), the formation age of the boundary between L-i<sub>NEJ</sub> and L-ii<sub>NEJ</sub> was 0.74–0.86 Ma, approximately coinciding with our suggestion that the increase in the influence of aeolian dust from L-ii<sub>NEJ</sub> to L-i<sub>NEJ</sub> was caused by the net increase in aeolian dust flux.

This study shows that the bulk (unleached) isotope composition of the Fe–Mn crusts is affected by the detritus, despite the significant difference in Sr concentration between Fe–Mn oxides and the detritus for detritus-rich Fe–Mn crusts (Figure 6). Such detritus-rich Fe–Mn crusts are reported from off NE Japan [27], off California [62], and the Arctic Ocean [47] and can reveal the temporal change in the influx and provenance of detrital materials using our method. In addition, our method can be applied to Fe–Mn nodules because Fe–Mn crusts and nodules comprise almost the same materials. Fe–Mn nodules can take in detrital materials, not only settling dust but also contacting sediment. Therefore, the application of our method to Fe–Mn nodules can identify sediments that Fe–Mn nodules contacted with or were sometimes buried in. Understanding the burial history of Fe–Mn nodules may elucidate why Fe–Mn nodules with slower growth and higher density than sediments can persist on sediment surfaces for millions of years.

Offshore of NE Japan, the Fe–Mn crust contains detritus from NE Japan and aeolian dust from China, which are marine sediment components in the same area [17]. Therefore, the detritus in the Fe–Mn crusts (and nodules growing on sediments) should be the same materials as the neighboring marine sediments. These sediments commonly contain clay minerals, such as smectite, illite, kaolinite, and chlorite [63]. Owing to the dissolution of chlorite and the release of elements from aluminosilicate clays in HCl [64], our results indicate that the HCl leaching of Fe–Mn crusts and nodules before the assessment of isotope compositions (e.g., [4,65,66]) should affect the estimation of the flux fractions of detritus contained in Fe–Mn crusts.

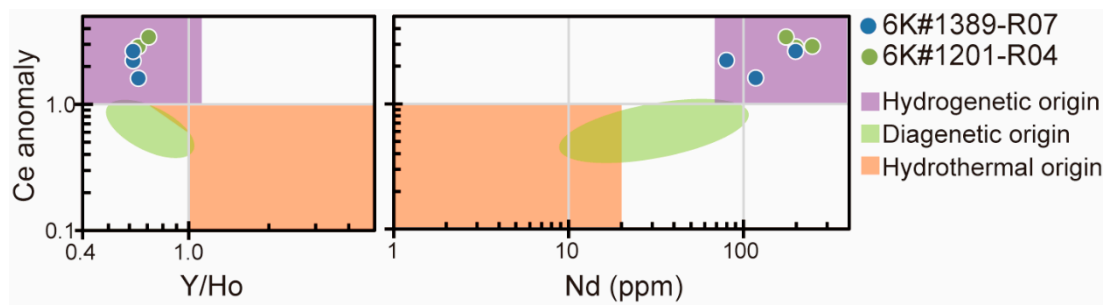


**Figure 5.** Discrimination plots of origins based on REEs. Fields of each origin are defined by Bau et al. [46]. Ce anomalies and Y/Ho ratios of the samples are normalized by Post Archean Australian Shale [67]. All samples are plotted in the hydrogenetic field.

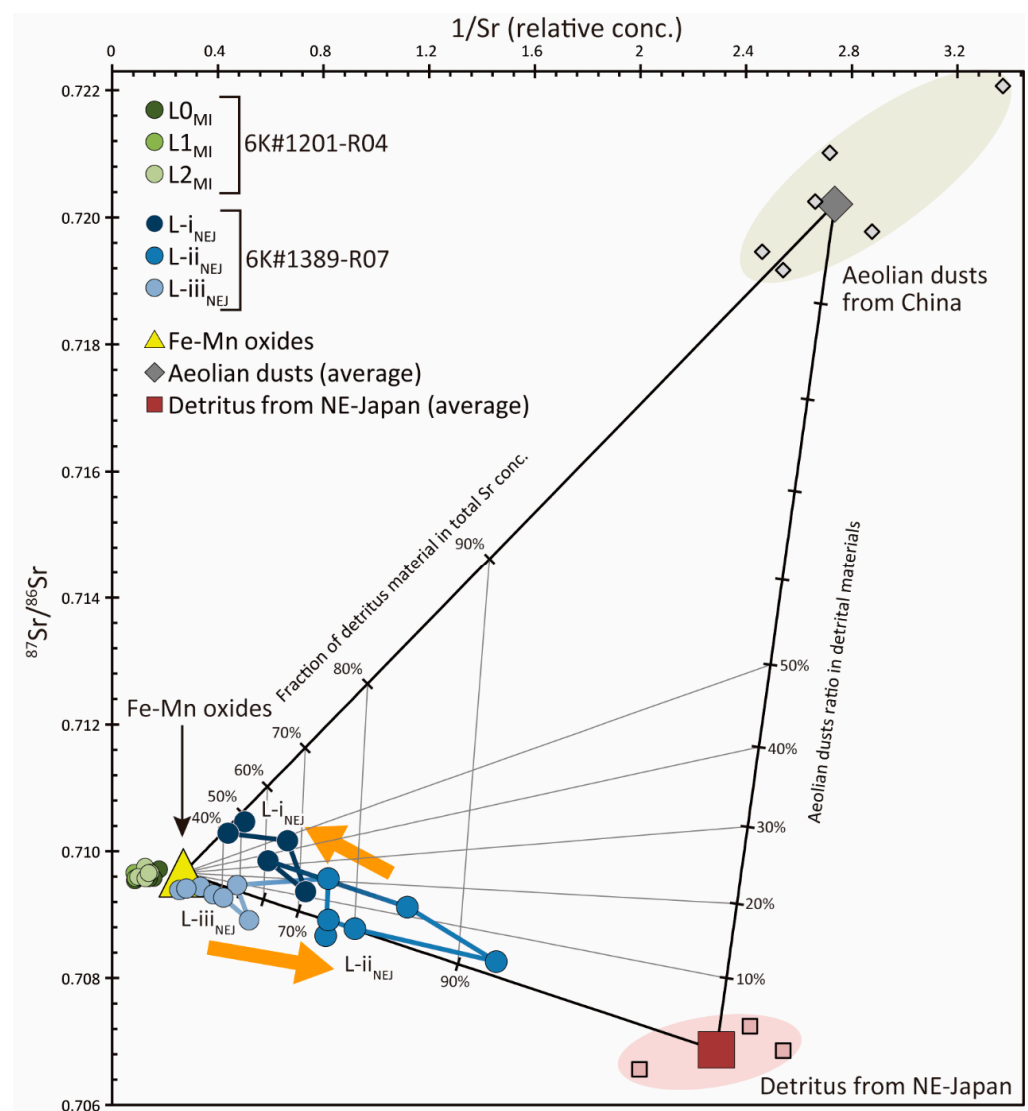


**Figure 6.** Three-component mix of Sr IR and relative Sr concentration. L-i<sub>NEJ</sub> to L-iii<sub>NEJ</sub> are connected from the inner to the outer side. The orange arrows indicate a general trend in the change from the inner to the outer layer. The details of the Fe–Mn oxides [15,55], aeolian dust from China [51], and the detritus from NE Japan [17] have been discussed in the main text.

**Table 5.** Average Sr content and IR of reference materials used in Figure 6.

	$^{87}\text{Sr}/^{86}\text{Sr}$	Sr ( $\mu\text{g/g}$ )	1/Sr (Relative Conc.)	n
Fe–Mn oxides [15,55]	0.70916	1451	0.270	1
Aeolian dusts from China [51]	0.719710456	143	2.742	6
Detritus from NE-Japan [17]	0.706367488	171	2.293	3
L-ii <sub>NEJ</sub>		415	0.945	6

## 5. Conclusions

To the best of our knowledge, this is the first study that reports the bulk (unleached) Sr IR of Fe–Mn crusts measured through LA-MC-ICP-MS to identify the provenances of detritus. Owing to the rapid uplift of the Ou backbone mountains, the L-iii<sub>NEJ</sub> and L-ii<sub>NEJ</sub> layers of the Fe–Mn crust from off NE Japan were affected by detritus from NE Japan. Thereafter, the influence of aeolian dust increased from the L-ii<sub>NEJ</sub> layer to the L-i<sub>NEJ</sub> layer, corresponding to the increase in aeolian dust flux due to global cooling in the Quaternary. Although LA-MC-ICP-MS is unsuitable for Fe–Mn crusts with a detritus fraction below 40% due to a large difference in Sr content between Fe–Mn oxides and detritus (Figure 6), it is useful for understanding the growth history of detritus-rich Fe–Mn crusts around the continental margin, such as off NE Japan (in this study and [27]), the Arctic Ocean [47], and off California [62].

The analysis of Sr IRs of Fe–Mn crusts via LA-MC-ICP-MS has allowed us to discuss the detritus provenances of the Fe–Mn crusts with higher time (spatial) resolution than that of previous studies (with >15 analysis/Myr in this study versus 1.2 analysis/Myr in a previous study [22]). The provenance investigation of detrital components in the Fe–Mn crusts can provide geological and paleoclimatology information, even across age intervals with marine sediment hiatus. Moreover, when LA-MC-ICP-MS is applied to Fe–Mn nodules that are constantly in contact with sediment that is buried, the burial history of Fe–Mn nodules may be revealed on the basis of the provenance of the contained detritus.

**Author Contributions:** Conceptualization, K.A. and N.H.; project administration, K.A. and N.H.; investigation, K.A., N.H., J.-I.K., Q.C., H.S., S.M. and K.Y.; resources, N.H., J.-I.K., Q.C., H.S., K.Y. and Y.K.; data curation, K.A. and N.H.; writing—original draft preparation, K.A.; writing—review and editing, all authors; visualization, K.A. and N.H.; funding acquisition, N.H. and Y.K. All authors have read and agreed to the published version of the manuscript.

**Funding:** This research was funded by the Japan Society for the Promotion of Science (JSPS) KAKENHI grant numbers JP17K05715 to N.H. and JP15H05771 to Y.K., and the Toray Science and Technology Grant (11-5208) to N.H.

**Data Availability Statement:** Not applicable.

**Acknowledgments:** The crew and scientific party of the *R/V Yokosuka* and the submersible *SHINKAI 6500* are thanked for collecting samples during the cruises YK10-05 and YK14-05. We thank T. Nozaki, JAMSTEC and K. Nakamura, from the University of Tokyo for helping with our analysis. The Institute for Integrated Radiation and Nuclear Science, Kyoto University, and the Isotope Science Center, University of Tokyo, are gratefully acknowledged for their assistance in undertaking the radiometric  $^{40}\text{Ar}/^{39}\text{Ar}$  dating.

**Conflicts of Interest:** The authors declare no conflict of interest.

## References

- Hein, J.R.; Koschinsky, A.; Bau, M.; Manheim, F.T.; Kang, J.K.; Roberts, L. Cobalt-Rich Ferromanganese Crusts in the Pacific. In *Handbook of Marine Mineral Deposits*; CRC Press: Boca Raton, FL, USA, 1999; pp. 239–281. ISBN 978-0849384295.
- Hu, R.; Chen, T.Y.; Ling, H.F. Late Cenozoic History of Deep Water Circulation in the Western North Pacific: Evidence from Nd Isotopes of Ferromanganese Crusts. *Chin. Sci. Bull.* **2012**, *57*, 4077–4086. [[CrossRef](#)]
- González, F.J.; Somoza, L.; Hein, J.R.; Medialdea, T.; León, R.; Urgan, V.; Reyes, J.; Martín-Rubí, J.A. Phosphorites, Co-Rich Mn Nodules, and Fe–Mn Crusts from Galicia Bank, NE Atlantic: Reflections of Cenozoic Tectonics and Paleooceanography. *Geochem. Geophys. Geosyst.* **2016**, *17*, 346–374. [[CrossRef](#)]

4. Wang, X.; Planavsky, N.J.; Reinhard, C.T.; Hein, J.R.; Johnson, T.M. A Cenozoic Seawater Redox Record Derived from  $^{238}\text{U}/^{235}\text{U}$  in Ferromanganese Crusts. *Am. J. Sci.* **2016**, *315*, 64–83. [[CrossRef](#)]
5. Nishi, K.; Usui, A.; Nakasato, Y.; Yasuda, H. Corrigendum to Formation Age of the Dual Structure and Environmental Change Recorded in Hydrogenetic Ferromanganese Crusts from Northwest and Central Pacific Seamounts. *Ore. Geol. Rev.* **2017**, *86*, 980. [[CrossRef](#)]
6. Marino, E.; González, F.J.; Somoza, L.; Lunar, R.; Ortega, L.; Vázquez, J.T.; Reyes, J.; Bellido, E. Strategic and Rare Elements in Cretaceous-Cenozoic Cobalt-Rich Ferromanganese Crusts from Seamounts in the Canary Island Seamount Province (Northeastern Tropical Atlantic). *Ore. Geol. Rev.* **2017**, *87*, 41–61. [[CrossRef](#)]
7. Koschinsky, A.; Halbach, P.; Hein, J.R.; Mangini, A. Ferromanganese Crusts as Indicators for Paleoceanographic Events in the NE Atlantic. *Geol. Rundsch.* **1996**, *85*, 567–576. [[CrossRef](#)]
8. Kuhn, T.; Bau, M.; Blum, N.; Halbach, P. Origin of Negative Ce Anomalies in Mixed Hydrothermal-Hydrogenetic Fe-Mn Crusts from the Central Indian Ridge. *Earth Planet. Sci. Lett.* **1998**, *163*, 207–220. [[CrossRef](#)]
9. Frank, M.; O’Nions, R.K.; Hein, J.R.; Banakar, V.K. 60 Myr Records of Major Elements and Pb-Nd Isotopes from Hydrogenous Ferromanganese Crusts: Reconstruction of Seawater Paleochemistry. *Geochim. Cosmochim. Acta* **1999**, *63*, 1689–1708. [[CrossRef](#)]
10. Goto, K.T.; Anbar, A.D.; Gordon, G.W.; Romaniello, S.J.; Shimoda, G.; Takaya, Y.; Tokumaru, A.; Nozaki, T.; Suzuki, K.; Machida, S.; et al. Uranium Isotope Systematics of Ferromanganese Crusts in the Pacific Ocean: Implications for the Marine  $^{238}\text{U}/^{235}\text{U}$  Isotope System. *Geochim. Cosmochim. Acta* **2014**, *146*, 43–58. [[CrossRef](#)]
11. Futa, K.; Peterman, Z.E.; Hein, J.R. Sr and Nd Isotopic Variations in Ferromanganese Crusts from the Central Pacific: Implications for Age and Source Provenance. *Geochim. Cosmochim. Acta* **1988**, *52*, 2229–2233. [[CrossRef](#)]
12. Ingram, B.; Hein, J.; Farmer, G. Age Determinations and Growth Rates of Pacific Ferromanganese Deposits Using Strontium Isotopes. *Geochim. Cosmochim. Acta* **1990**, *54*, 1709–1721. [[CrossRef](#)]
13. Ito, T.; Usui, A.; Kajiwara, Y.; Nakano, T. Strontium Isotopic Compositions and Paleoceanographic Implication of Fossil Manganese Nodules in DSDP/ODP Cores, Leg 1-126. *Geochim. Cosmochim. Acta* **1998**, *62*, 1545–1554. [[CrossRef](#)]
14. Henderson, G.M.; Burton, K.W. Using ( $^{234}\text{U}/^{238}\text{U}$ ) to Assess Diffusion Rates of Isotope Tracers in Ferromanganese Crusts. *Earth Planet. Sci. Lett.* **1999**, *170*, 169–179. [[CrossRef](#)]
15. McArthur, J.; Sahami, A.; Thirlwall, M.; Hamilton, P.; Osborn, A. Dating Phosphogenesis with Strontium Isotopes. *Geochim. Cosmochim. Acta* **1990**, *54*, 1343–1351. [[CrossRef](#)]
16. Amakawa, H.; Ingri, J.; Masuda, A.; Shimizu, H. Isotopic Compositions of Ce, Nd and Sr in Ferromanganese Nodules from the Pacific and Atlantic Oceans, the Baltic and Barents Seas, and the Gulf of Bothnia. *Earth Planet. Sci. Lett.* **1991**, *105*, 554–565. [[CrossRef](#)]
17. Asahara, Y.; Tanaka, T.; Kamioka, H.; Nishimura, A. Asian Continental Nature of  $^{87}\text{Sr}/^{86}\text{Sr}$  Ratios in North Central Pacific Sediments. *Earth Planet. Sci. Lett.* **1995**, *133*, 105–116. [[CrossRef](#)]
18. Asahara, Y.  $^{87}\text{Sr}/^{86}\text{Sr}$  Variation in North Pacific Sediments: A Record of the Milankovitch Cycle in the Past 3 Million Years. *Earth Planet. Sci. Lett.* **1999**, *171*, 453–464. [[CrossRef](#)]
19. Zhang, W.; Chen, J.; Ji, J.; Li, G. Evolving Flux of Asian Dust in the North Pacific Ocean since the Late Oligocene. *Aeolian Res.* **2016**, *23*, 11–20. [[CrossRef](#)]
20. Hein, J.R.; Yeh, H.-W.; Gunn, S.H.; Sliter, W.V.; Benninger, L.M.; Wang, C.-H. Two Major Cenozoic Episodes of Phosphogenesis Recorded in Equatorial Pacific Seamount Deposits. *Paleoceanography* **1993**, *8*, 293–311. [[CrossRef](#)]
21. Hyeong, K.; Kim, J.; Yoo, C.M.; Moon, J.-W.; Seo, I. Cenozoic History of Phosphogenesis Recorded in the Ferromanganese Crusts of Central and Western Pacific Seamounts: Implications for Deepwater Circulation and Phosphorus Budgets. *Palaeogeogr. Palaeoclimatol. Palaeoecol.* **2013**, *392*, 293–301. [[CrossRef](#)]
22. Banakar, V.K.; Galy, A.; Sukumaran, N.P.; Parthiban, G.; Volvaiker, A.Y. Himalayan Sedimentary Pulses Recorded by Silicate Detritus within a Ferromanganese Crust from the Central Indian Ocean. *Earth Planet. Sci. Lett.* **2003**, *205*, 337–348. [[CrossRef](#)]
23. Bolhão Muiños, S. *Ferromanganese Crusts from the Seamounts North of the Madeira Island: Composition, Origin and Paleoceanographic Conditions*; Kiel University: Kiel, Germany, 2015.
24. González, F.J.; Somoza, L.; León, R.; Medialdea, T.; de Torres, T.; Ortiz, J.E.; Lunar, R.; Martínez-Frías, J.; Merinero, R. Ferromanganese Nodules and Micro-Hardgrounds Associated with the Cadiz Contourite Channel (NE Atlantic): Palaeoenvironmental Records of Fluid Venting and Bottom Currents. *Chem. Geol.* **2012**, *310–311*, 56–78. [[CrossRef](#)]
25. Hirano, N.; Takahashi, E.; Yamamoto, J.; Abe, W.; Ingle, S.P.; Kaneoka, I.; Hirata, T.; Kimura, J.I.; Ishii, T.; Ogawa, Y.; et al. Volcanism in Response to Plate Flexure. *Science* **2006**, *313*, 1426–1428. [[CrossRef](#)] [[PubMed](#)]
26. Hirano, N.; Machida, S. The Mantle Structure below Petit-Spot Volcanoes. *Commun. Earth Environ.* **2022**, *3*, 110. [[CrossRef](#)]
27. Azami, K.; Hirano, N.; Machida, S.; Yasukawa, K.; Kato, Y. Rare Earth Elements and Yttrium (REY) Variability with Water Depth in Hydrogenetic Ferromanganese Crusts. *Chem. Geol.* **2018**, *493*, 224–233. [[CrossRef](#)]
28. Yamamoto, S. Dissolution and Diagenesis of Deep-Sea Carbonates in Some Trench Basins of the Western Pacific. *Carbonates Evaporites* **1988**, *3*, 107–123. [[CrossRef](#)]
29. Sato, Y.; Hirano, N.; Machida, S.; Yamamoto, J.; Nakanishi, M.; Ishii, T.; Taki, A.; Yasukawa, K.; Kato, Y. Direct Ascent to the Surface of Asthenospheric Magma in a Region of Convex Lithospheric Flexure. *Int. Geol. Rev.* **2018**, *60*, 1231–1243. [[CrossRef](#)]

30. Kimura, J.-I.; Takahashi, T.; Chang, Q. A New Analytical Bias Correction for in Situ Sr Isotope Analysis of Plagioclase Crystals Using Laser-Ablation Multiple-Collector Inductively Coupled Plasma Mass Spectrometry. *J. Anal. At. Spectrom.* **2013**, *28*, 945. [[CrossRef](#)]
31. Kato, Y.; Fujinaga, K.; Suzuki, K. Major and Trace Element Geochemistry and Os Isotopic Composition of Metalliferous Umbers from the Late Cretaceous Japanese Accretionary Complex. *Geochem. Geophys. Geosyst.* **2005**, *6*, Q07004. [[CrossRef](#)]
32. Makishima, A.; Nakamura, E. Determination of Major/ Minor and Trace Elements in Silicate Samples by ICP-QMS and ICP-SFMS Applying Isotope Dilution-Internal Standardisation (ID-IS) and Multi-Stage Internal Standardisation. *Geostand. Geanal. Res.* **2006**, *30*, 245–271. [[CrossRef](#)]
33. Takaya, Y.; Hiraide, T.; Fujinaga, K.; Nakamura, K.; Kato, Y. A Study on the Recovery Method of Rare-Earth Elements from REY-Rich Mud toward the Development and the Utilization of REY-Rich Mud. *J. MMIJ* **2014**, *130*, 104–114. [[CrossRef](#)]
34. Iwata, N. *Geochronological Study of the Deccan Volcanism by the <sup>40</sup>Ar-<sup>39</sup>Ar Method*; The University of Tokyo: Tokyo, Japan, 1998.
35. Saito, K. Excess Ar in Some Metamorphic and Plutonic Rocks and Reduction of Thermal Neutron-Induced <sup>40</sup>Ar by Cd Shielding. *Sci. Rep. Res. Inst. Tohoku Univ. Ser. A Phys. Chem. Metall.* **1994**, *40*, 185–189.
36. Ebisawa, N.; Sumino, H.; Okazaki, R.; Takigami, Y.; Hirano, N.; Nagao, K.; Kaneoka, I. Construction of I-Xe and <sup>40</sup>Ar-<sup>39</sup>Ar Dating System Using a Modified VG3600 Mass Spectrometer and the First I-Xe Data Obtained in Japan. *J. Mass Spectrom. Soc. Jpn.* **2004**, *52*, 219–229. [[CrossRef](#)]
37. Wessel, P.; Smith, W.H.F. Free Software Helps Map and Display Data. *Eos Trans. Am. Geophys. Union* **1991**, *72*, 441–446. [[CrossRef](#)]
38. Wessel, P.; Smith, W.H.F.; Scharroo, R.; Luis, J.; Wobbe, F. Generic Mapping Tools: Improved Version Released. *Eos (Wash. DC)*. **2013**, *94*, 409–410. [[CrossRef](#)]
39. Amante, C.; Eakins, B.W. ETOPO1 1 Arc-Minute Global Relief Model: Procedures, Data Sources and Analysis. In Proceedings of the NOAA Technical Memorandum NESDIS NGDC-24; 2009; p. 19. [[CrossRef](#)]
40. Machida, S.; Fujinaga, K.; Ishii, T.; Nakamura, K.; Hirano, N.; Kato, Y. Geology and Geochemistry of Ferromanganese Nodules in the Japanese Exclusive Economic Zone around Minamitorishima Island. *Geochem. J.* **2016**, *50*, 539–555. [[CrossRef](#)]
41. Usui, A.; Mellin, T.A.; Nohara, M.; Yuasa, M. Structural Stability of Marine 10 Å Manganates from the Ogasawara (Bonin) Arc: Implication for Low-Temperature Hydrothermal Activity. *Mar. Geol.* **1989**, *86*, 41–56. [[CrossRef](#)]
42. Marino, E.; González, F.J.; Lunar, R.; Reyes, J.; Medialdea, T.; Castillo-Carrión, M.; Bellido, E.; Somoza, L. High-Resolution Analysis of Critical Minerals and Elements in Fe–Mn Crusts from the Canary Island Seamount Province (Atlantic Ocean). *Minerals* **2018**, *8*, 285. [[CrossRef](#)]
43. Marino, E.; González, F.J.; Kuhn, T.; Madureira, P.; Wegorzewski, A.V.; Mirao, J.; Medialdea, T.; Oeser, M.; Miguel, C.; Reyes, J.; et al. Hydrogenetic, Diagenetic and Hydrothermal Processes Forming Ferromanganese Crusts in the Canary Island Seamounts and Their Influence in the Metal Recovery Rate with Hydrometallurgical Methods. *Minerals* **2019**, *9*, 439. [[CrossRef](#)]
44. Brent Dalrymple, G.; Lanphere, M.A. <sup>40</sup>Ar/<sup>39</sup>Ar Age Spectra of Some Undisturbed Terrestrial Samples. *Geochim. Cosmochim. Acta* **1974**, *38*, 715–738. [[CrossRef](#)]
45. Koppers, A.A.P.; Staudigel, H.; Wijbrans, J.R. Dating Crystalline Groundmass Separates of Altered Cretaceous Seamount Basalts by the <sup>40</sup>Ar/<sup>39</sup>Ar Incremental Heating Technique. *Chem. Geol.* **2000**, *166*, 139–158. [[CrossRef](#)]
46. Bau, M.; Schmidt, K.; Koschinsky, A.; Hein, J.; Kuhn, T.; Usui, A. Discriminating between Different Genetic Types of Marine Ferro-Manganese Crusts and Nodules Based on Rare Earth Elements and Yttrium. *Chem. Geol.* **2014**, *381*, 1–9. [[CrossRef](#)]
47. Hein, J.R.; Konstantinova, N.; Mikesell, M.; Mizell, K.; Fitzsimmons, J.N.; Lam, P.J.; Jensen, L.T.; Xiang, Y.; Gartman, A.; Cherkashov, G.; et al. Arctic Deep Water Ferromanganese-Oxide Deposits Reflect the Unique Characteristics of the Arctic Ocean. *Geochem. Geophys. Geosyst.* **2017**, *18*, 3771–3800. [[CrossRef](#)]
48. Boyden, J.A.; Müller, R.D.; Gurnis, M.; Torsvik, T.H.; Clark, J.A.; Turner, M.; Ivey-Law, H.; Watson, R.J.; Cannon, J.S. Next-Generation Plate-Tectonic Reconstructions Using GPlates. In *Geoinformatics*; Keller, G.R., Baru, C., Eds.; Cambridge University Press: Cambridge, MA, USA, 2011; pp. 95–114. ISBN 9780521897150.
49. Matthews, K.J.; Maloney, K.T.; Zahirovic, S.; Williams, S.E.; Seton, M.; Müller, R.D. Global Plate Boundary Evolution and Kinematics since the Late Paleozoic. *Glob. Planet. Chang.* **2016**, *146*, 226–250. [[CrossRef](#)]
50. Farrell, J.W.; Clemens, S.C.; Peter Gromet, L. Improved Chronostratigraphic Reference Curve of Late Neogene Seawater <sup>87</sup>Sr/<sup>86</sup>Sr. *Geology* **1995**, *23*, 403. [[CrossRef](#)]
51. Yokoo, Y.; Nakano, T.; Nishikawa, M.; Quan, H. Mineralogical Variation of Sr-Nd Isotopic and Elemental Compositions in Loess and Desert Sand from the Central Loess Plateau in China as a Provenance Tracer of Wet and Dry Deposition in the Northwestern Pacific. *Chem. Geol.* **2004**, *204*, 45–62. [[CrossRef](#)]
52. Chen, J.; An, Z.; Liu, L.; Ji, J.; Yang, J.; Chen, Y. Variations in Chemical Compositions of the Eolian Dust in Chinese Loess Plateau over the Past 2.5 Ma and Chemical Weathering in the Asian Inland. *Sci. China Ser. D Earth Sci.* **2001**, *44*, 403–413. [[CrossRef](#)]
53. Miyazaki, T.; Kimura, J.-I.; Katakuse, M. Geochemical Records from Loess Deposits in Japan over the Last 210 Kyr: Lithogenic Source Changes and Paleoclimatic Indications. *Geochem. Geophys. Geosyst.* **2016**, *17*, 2745–2761. [[CrossRef](#)]
54. Minami, M. *Geochemical Map of Strontium Isotope Ratio in Japan: A Database for Tracing of Ancient Human Migration and Archeological Remains Transport, Report of the Grant-in-Aid for Scientific Research*; No. 22300308; Scientific Research Publishing: Wuhan, China, 2015.
55. Koschinsky, A.; Hein, J.R. Uptake of Elements from Seawater by Ferromanganese Crusts: Solid-Phase Associations and Seawater Speciation. *Mar. Geol.* **2003**, *198*, 331–351. [[CrossRef](#)]

56. Taira, A. Tectonic Evolution of the Japanese Island Arc System. *Annu. Rev. Earth Planet. Sci.* **2001**, *29*, 109–134. [[CrossRef](#)]
57. Nakajima, T.; Danhara, T.; Iwano, H.; Chinzei, K. Uplift of the Ou Backbone Range in Northeast Japan at around 10 Ma and Its Implication for the Tectonic Evolution of the Eastern Margin of Asia. *Palaeogeogr. Palaeoclimatol. Palaeoecol.* **2006**, *241*, 28–48. [[CrossRef](#)]
58. Sueoka, S.; Tagami, T.; Kohn, B.P. First Report of (U–Th)/He Thermochronometric Data across Northeast Japan Arc: Implications for the Long-Term Inelastic Deformation. *Earth Planets Sp.* **2017**, *69*, 79. [[CrossRef](#)]
59. Togashi, S.; Imai, N.; Okuyama-Kusunose, Y.; Tanaka, T.; Okai, T.; Koma, T.; Murata, Y. Young Upper Crustal Chemical Composition of the Orogenic Japan Arc. *Geochem. Geophys. Geosyst.* **2000**, *1*. [[CrossRef](#)]
60. Ohta, A.; Imai, N.; Tachibana, Y.; Ikehara, K.; Katayama, H.; Nakajima, T. Influence of Different Sedimentary Environments on Multi-Elemental Marine Geochemical Maps of the Pacific Ocean and Sea of Japan, Tohoku Region. *Bull. Geol. Surv. Jpn.* **2017**, *68*, 87–110. [[CrossRef](#)]
61. Hovan, S.A.; Rea, D.K.; Pisias, N.G.; Shackleton, N.J. A Direct Link between the China Loess and Marine  $\Delta 18\text{O}$  Records: Aeolian Flux to the North Pacific. *Nature* **1989**, *340*, 296–298. [[CrossRef](#)]
62. Conrad, T.; Hein, J.R.; Paytan, A.; Clague, D.A. Formation of Fe–Mn Crusts within a Continental Margin Environment. *Ore Geol. Rev.* **2017**, *87*, 25–40. [[CrossRef](#)]
63. Rateev, M.A.; Gorbunova, Z.N.; Lisitzyn, A.P.; Nosov, G.L. The Distribution of Clay Minerals in the Oceans. *Sedimentology* **1969**, *13*, 21–43. [[CrossRef](#)]
64. Steel, K.M.; Besida, J.; O'Donnell, T.A.; Wood, D.G. Production of Ultra Clean Coal-Part II-Ionic Equilibria in Solution When Mineral Matter from Black Coal Is Treated with Aqueous Hydrofluoric Acid. *Fuel Process. Technol.* **2001**, *70*, 193–219. [[CrossRef](#)]
65. David, K.; Frank, M.; O'Nions, R.K.; Belshaw, N.S.; Arden, J.W. The Hf Isotope Composition of Global Seawater and the Evolution of Hf Isotopes in the Deep Pacific Ocean from Fe–Mn Crusts. *Chem. Geol.* **2001**, *178*, 23–42. [[CrossRef](#)]
66. Amakawa, H.; Usui, A.; Iijima, K.; Suzuki, K. Surface Layer Nd Isotopic Composition of Ferromanganese Crusts Collected from the Takuyo-Daigo Seamount Reflects Ambient Seawater. *Geochem. J.* **2017**, *51*, e1–e7. [[CrossRef](#)]
67. Taylor, S.R.; McLennan, S.M. *The Continental Crust: Its Composition and Evolution*; Geoscience Texts; Blackwell Scientific Publications: Oxford, UK, 1985; ISBN 0632011483.